

Extraordinary Areal and Volumetric Performance of Flexible Solid-State Micro-Supercapacitors Based on Highly Conductive Freestanding $\text{Ti}_3\text{C}_2\text{T}_x$ Films

Haichao Huang, Hai Su, Haitao Zhang,* Ludi Xu, Xiang Chu, Chunfeng Hu, Huan Liu, Ningjun Chen, Fangyan Liu, Wen Deng, Bingni Gu, Hepeng Zhang, and Weiqing Yang*

Approaching state-of-the-art areal and volumetric capacitances while maintaining high-power characteristic is a big challenge that promotes practical application of flexible solid-state micro-supercapacitors (MSCs), which have recently attracted great attention with the rapid development of flexible microelectronics. Herein, it is reported that freestanding extrahigh conductive $\text{Ti}_3\text{C}_2\text{T}_x$ (MXene) films with excellent flexibility and effectively controlled thickness ranging from 1–21 μm performed as excellently scalable and flexible solid-state MSCs owing to their ultrahigh underlying electrical conductivity (up to $1.25 \times 10^5 \text{ S m}^{-1}$) and self-functionalized surfaces (O, OH, and F terminations). Amazingly, freestanding conductive $\text{Ti}_3\text{C}_2\text{T}_x$ based flexible solid-state MSCs with interdigital electrodes and polyvinyl alcohol/sulfuric acid (PVA/ H_2SO_4) gel electrolyte display outstanding areal capacitances of 340 mF cm^{-2} at 0.25 mA cm^{-2} based on the two working electrodes. Moreover, the maximum corresponding volumetric capacitance and energy density of flexible solid-state MSCs reach up to 183 F cm^{-3} and 12.4 mWh cm^{-3} , which is on the topmost level among all the unconventional supercapacitors to date. Compared with materials currently used in MSCs, this freestanding conductive $\text{Ti}_3\text{C}_2\text{T}_x$ shows potential and scalability in increasing overall micro-supercapacitor performance, which evidently sheds light on promising application of freestanding conductive MXenes for next-generation flexible, portable, and integrated MSCs.

as well as light-weight, remarkable flexibility, and security.^[1–5] During last 5–7 years, we witnessed the rapid improvement of unconventional supercapacitors including high-performance (especially the areal and volumetric properties) supercapacitors,^[6–9] novel structured micro-supercapacitors,^[10–12] ultrathin and transparent devices,^[13,14] flexible all-solid-state supercapacitors,^[15–19] and on-chip and large-scale integrated micro-supercapacitors.^[20–22] Although these breakthroughs were made, development of MSCs is still in its infancy. And lots of importance and challenges such as 3D architecture design, high-conductive leakage-free electrolytes, low self-discharge effect, large-scale on-chip integration at microscale, high mechanical reliability, and outstanding performances in areal and volumetric need to be further addressed. Similar to conventional supercapacitors with inflexibility and liquid electrolytes, the intrinsic properties of the electrode materials, which are critical to high-performance supercapacitors and the method of electrode fabrication, evidently play the most important role in developing

1. Introduction

Since the rapidly increasing demand for miniaturized portable, wearable, and integrated electronics, flexible micro-supercapacitors (MSCs) have been considered as promising power sources owing to their superior power characteristic

state-of-the-art MSCs. In this respect, it is the key to find one material that possesses both outstanding mechanical flexibility and electrochemical performance.

MXenes, one kind of novel 2D materials, are promising candidates for developing state-of-the-art MSCs because of their outstanding electrical conductivity, superior areal and

H. Huang, H. Su, Dr. H. Zhang, X. Chu, N. Chen, F. Liu, W. Deng, B. Gu, H. Zhang, Prof. W. Yang
 Key Laboratory of Advanced Technologies of Materials
 (Ministry of Education)
 School of Materials Science and Engineering
 Southwest Jiaotong University
 Chengdu, Sichuan 610031, China
 E-mail: haitaozhang@swjtu.edu.cn; wqyang@swjtu.edu.cn

L. Xu, Dr. C. Hu
 State Key Laboratory of Traction Power
 School of Materials Science and Engineering
 Southwest Jiaotong University
 Chengdu, Sichuan 610031, China
 H. Liu
 State Key Laboratory of Silicon Materials
 Department of Materials Science and Engineering
 Zhejiang University
 Hangzhou, Zhejiang 310027, China

 The ORCID identification number(s) for the author(s) of this article can be found under <https://doi.org/10.1002/aelm.201800179>.

DOI: 10.1002/aelm.201800179

volumetric capacitance, and mechanical flexibility. So far, more than 20 different MXenes have been experimentally synthesized, including Ti_3C_2 , Mo_2C , Sc_2C , Ti_2C , Nb_4C_3 , Nb_2C , V_2C , Cr_2C , and so on.^[23] The chemical formula of these materials can be represented by $\text{M}_{n+1}\text{X}_n\text{T}_x$, where M refers to early transition metals (such as Ti, Zr, Hf, V, Nb, Ta, Cr, Sc, etc.), X refers to C or/and N, n is generally 1, 2, or 3, and T_x represents surface groups (such as O^{2-} , OH^- , F^-).^[24–28] $\text{Ti}_3\text{C}_2\text{T}_x$ is the first and also the most studied MXene for energy storage application.^[3] Compared with other capacitive materials, 2D $\text{Ti}_3\text{C}_2\text{T}_x$ did not only have ultrahigh electrical conductivities, but also exhibited an ultrahigh volumetric capacitance.^[29,30] In addition, freestanding MXene films with outstanding flexibility can be easily obtained by vacuum-assisted filtration. Nevertheless, there are few studies about MXenes-based flexible solid-state MSCs. Ghidui et al. demonstrated the fabrication of an MXene-based micro-supercapacitor with a low volumetric capacitance of only 14.4 F cm^{-3} in H_3PO_4 electrolyte.^[31] And more recently, Gogotsi and co-workers reported solid-state MXene-based micro-supercapacitors owing an areal capacitance of 27 mF cm^{-2} with ultrahigh volumetric capacitance.^[17]

Herein we report that the scalable and flexible solid-state MSCs based on highly conductive freestanding MXene films deliver ultrahigh areal and volumetric properties. The in-plane interdigitated micro-supercapacitors constructed with freestanding $\text{Ti}_3\text{C}_2\text{T}_x$ film electrodes and polyvinyl alcohol/sulfuric acid (PVA/ H_2SO_4) gel electrolyte show high areal capacitance up to 340 mF cm^{-2} and ultrahigh volumetric capacitance of 183 F cm^{-3} at 0.25 mA cm^{-2} based on the two-electrodes (the corresponding 1360 mF cm^{-2} and 732 F cm^{-3} for one single electrode), which are higher than most of the reported MXene based MSCs, more importantly, 1–2 orders higher than other

unconventional supercapacitors based on graphene, carbon nanotubes, and porous carbons electrodes.^[9,32,33] Moreover, the freestanding highly conductive $\text{Ti}_3\text{C}_2\text{T}_x$ films with effectively controlled thickness ranging widely from 1 to $21 \mu\text{m}$ and good flexibility are directly vacuum filtrated through solution processable aqueous ink. This massive production method in combination with simplified device manufactured process and uncomplicated encapsulation technology unambiguously guarantees the potential application of freestanding highly conductive MXene films and hence opens up a new approach for high performance energy storage devices application in integrated energy management electronics. Therefore, this ultrahigh conductive freestanding $\text{Ti}_3\text{C}_2\text{T}_x$ MXene film will potentially pave the way for massive manufacture of flexible solid-state micro-supercapacitor with excellent practical areal and volumetric performance.

2. Results and Discussion

To clearly demonstrate the derivation of the freestanding MXene films, its preparation process by chemical etch of ceramic powders and vacuum filtration was schematically presented in **Figure 1**. Ti_3AlC_2 powders, one of the bulk ternary layered carbides and nitrides (MAX phase) ceramic with ternary-layered structure (Figure 1a), were chemically etched under concentrated HCl and LiF solution to obtain 2D $\text{Ti}_3\text{C}_2\text{T}_x$ ($T = \text{H}, \text{O}, \text{F}$), as shown in Figure 1b. And that, due to hydrophilic heteroatoms functionalization, these MXenes, with the help of mild sonication, can fully form well-dispersed colloidal aqueous solution as proved by apparent Tyndall effect (Figure 1c). Here, this kind of stable colloidal solution is strong guarantee of uniform MXene membrane (Figure 1d) supported

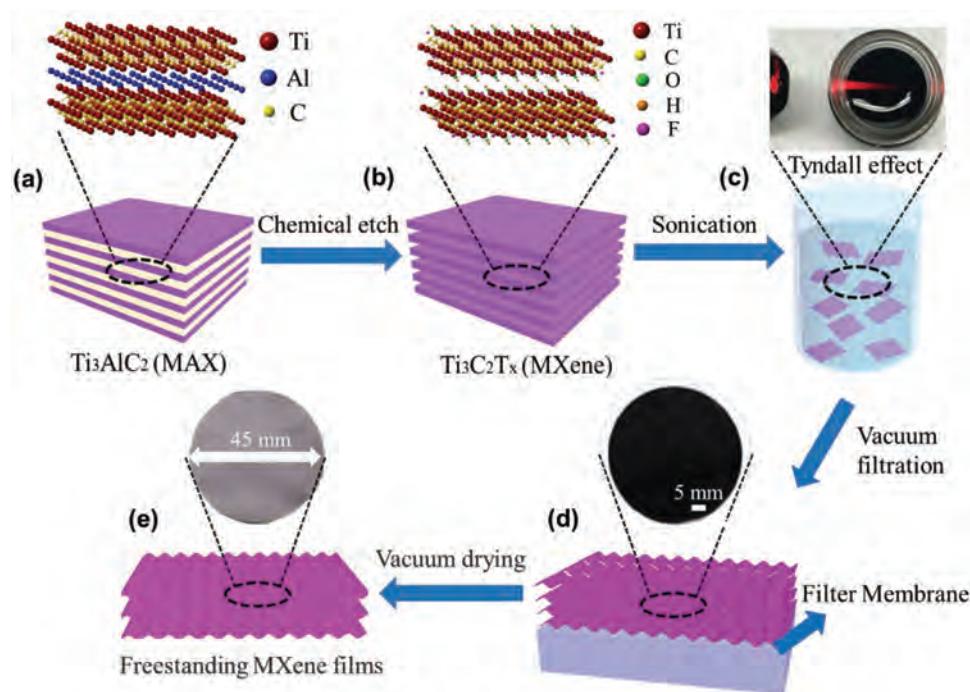


Figure 1. Schematic illustration of the synthetic route. a) The Ti_3AlC_2 MAX phase with layered structure. Preparation of the b,c) MXene colloidal aqueous solution by b) chemical etch and c) sonication, d) filter membrane supported MXene films and e) freestanding conductive MXene films.

on the filter substrate through simply vacuum filtration. After further vacuum drying, freestanding MXene films as displayed in Figure 1e were successfully prepared by peeling off the substrates. The obtained freestanding MXene films confidently possess ultrahigh electric conductivity up to $1.25 \times 10^5 \text{ S m}^{-1}$ and sheet resistance of $0.015 \Omega \square^{-1}$ confirmed by four-point probe method (Table S1 and Figure S1, Supporting Information). Such a high electric conductivity is identified as one of the important factors for high-power MSCs.^[29]

After etching for 45 h, this product was well stratified as the scanning electron microscope (SEM) image shown (Figure 2a). Most of the exfoliated MXene sheets with lateral size of several micrometers keep layered structure similar to $\text{Ti}_3\text{C}_2\text{T}_x$ MAX precursors (Figures S2 and S3, Supporting Information). Typical transmission electron microscopy (TEM) micrographs of $\text{Ti}_3\text{C}_2\text{T}_x$ MXene flakes were shown in Figure 2b,c. Flat feature

with wrinkling for MXene platelets was observed (Figure 2b). Figure 2c shows the two-layer defect-free $\text{Ti}_3\text{C}_2\text{T}_x$ flakes and the corresponding interlayer spacing dramatically broadens to be 2.04 nm, which is much larger than that of previously reported untreated $\text{Ti}_3\text{C}_2\text{T}_x$ with an interlayer spacing of $\approx 1.0 \text{ nm}$.^[30,35–37] Such an interlayer spacing renders more available ionic accommodation and strongly safeguards the extrahigh areal and volumetric capacitances. On the contrary, the $\text{Ti}_3\text{C}_2\text{T}_x$ flakes with sonication treatment show much more defects and smaller lateral dimension which may decrease the conductivity (Figure S4, Supporting Information), dramatically lowering the power density of MSCs.^[38]

Freestanding $\text{Ti}_3\text{C}_2\text{T}_x$ films with wrinkles have been obtained by vacuum-assisted filtration, as shown in Figure 2d. Simultaneously, excellent flexibility of the films can be perceived by bending the films, as the digital photograph shows (the inset of

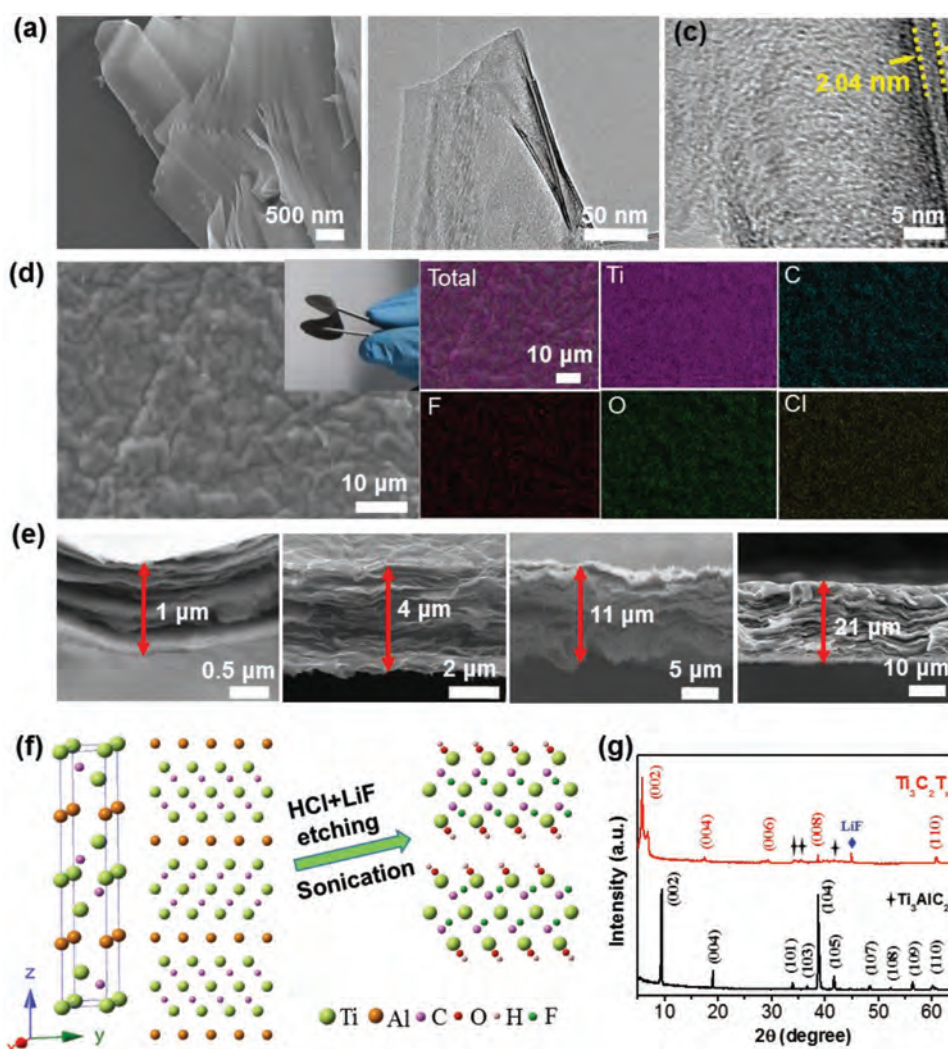


Figure 2. Morphology and structure of MXene platelets and thickness-controlled freestanding films. Representative a) Field emission scanning electron microscopy (FE-SEM), b) TEM, and c) HRTEM images of MXene platelets. d) Representative FE-SEM and EDX mapping of MXene films. Left inset: the prepared MXene films show excellent flexibility after bending. Right: the uniform elemental distribution. e) Representative FE-SEM images of MXene films with different thicknesses. From left to right: $1.0 \pm 0.1 \mu\text{m}$, $4.0 \pm 0.1 \mu\text{m}$, $11.0 \pm 0.1 \mu\text{m}$, and $21.0 \pm 0.1 \mu\text{m}$. f) Schematic illustrations of converting 3D Ti_3AlC_2 into 2D $\text{Ti}_3\text{C}_2\text{T}_x$ ($x = \text{F}, \text{O}, \text{and H}$). Left: the crystal structure of Ti_3AlC_2 . Middle: the atomic arrangement along (1 0 0) facet. Right: the atomic arrangement of functionalized $\text{Ti}_3\text{C}_2\text{T}_x$ along (1 0 0) facet. g) XRD pattern of $\text{Ti}_3\text{C}_2\text{T}_x$ film. XRD pattern of precursor Ti_3AlC_2 are also given for comparing.

Figure 2d). According to the energy dispersive X-ray (EDX) spectroscopy analysis (Figure 2e), Ti, C are the main elements, and O, F occupy a smaller proportion at the same time, which can yield the evident conclusion that the Al atom layer was mostly removed from Ti_3AlC_2 phase. The exactly atomic percentages of MXene films are summarized in Table S2 (Supporting Information). We proved that the thickness could be adjusted via changing the mass of the Ti_3AlC_2 colloidal solution. As the cross-section SEM shown, different film thicknesses ranging widely from 1 to 21 μm were obtained (Figure 2e), evidently demonstrating the excellent scalability and controllability of as-prepared MXene films. And the digital photographs of the corresponding thickness films were also shown in Figure S5 (Supporting Information). Therefore, this kind of simply controlling thickness method of freestanding conductive thin film will promote the massive production of the similar functional thin films.

In the Ti_3AlC_2 structure, the C atoms fill in the octahedral voids formed by the Ti atoms and the Ti–C layers are separated by the Al atoms layer (Figure 2f). After etching the Al atoms out of the crystal structure, the shift of (0 0 2) peak at $2\theta = 9.5^\circ$ to lower angle ($2\theta = 6.5^\circ$) and the disappearance of the most intense diffraction peak of Ti_3AlC_2 at $2\theta = 39^\circ$ in the X-ray diffraction (XRD) patterns obviously indicate that the Ti_3AlC_2 is successfully converted into $\text{Ti}_3\text{C}_2\text{T}_x$ (Figure S6, Supporting Information). One apparent diffraction peak occurred at $\approx 45^\circ$ may be originated from LiF phase because of the layered structure of MXenes and low water solubility of LiF. And some much smaller noise peaks may be originated from the remained little Ti_3AlC_2 precursor or the incompletely smooth MXene films caused the vibration of baseline during

XRD characterization. These exfoliated $\text{Ti}_3\text{C}_2\text{T}_x$ nanosheets are very important to achieve high-quality MXene membranes that show no apparent restack in their preferred orientation as indicated by XRD pattern (Figure 2g).

For a systematical characterization of as-prepared MXene film, Raman spectra and X-ray photoelectron spectroscopy (XPS) measurements performed on freestanding MXene membranes were carried out to identify the various chemical and termination species. In Figure 3a, the MXene films show five to six phonon spectral peaks with the Raman shifts ranging from 100 to 800 cm^{-1} and the exact peak positions are summarized in Table S3 (Supporting Information). According to the previous works,^[4,39] the mode at 728 cm^{-1} softened from pure Ti_3C_2 can be assigned to the out-of-plane vibrations of C atoms in $\text{Ti}_3\text{C}_2\text{O}_2$. After terminated by O, F, and OH heteroatoms, the out-of-plane stretching vibrations of Ti_2 are also softened to $\approx 203.8 \text{ cm}^{-1}$ for all the $\text{Ti}_3\text{C}_2\text{T}_x$ membranes. In fact, it is worth noting that the presence of oxygen-containing groups results in an obvious increase in capacitance.^[17]

For freestanding MXene films, the out-of-plane motion of surface Ti_2 is weakened but the out-of-plane vibration of C atoms is strengthened by the termination, which is similar to MXene monolayer.^[39] Herein the terminal groups are actually heterogeneous as forms of $\text{Ti}_3\text{C}_2\text{O}_2$ and $\text{Ti}_3\text{C}_2(\text{OH})_2$, which is clearly implied by the bimodal vibration located at around 600 cm^{-1} . One peak locating at lower wavenumber of 584.8 cm^{-1} is assigned to $\text{Ti}_3\text{C}_2\text{O}_2$ while the other at higher wavenumber of 622 cm^{-1} originates from $\text{Ti}_3\text{C}_2(\text{OH})_2$. The heterogeneous terminal groups can be further reflected by a broad responsive peak at about 385.6 cm^{-1} for the freestanding MXene membranes. However, since water trapped between the

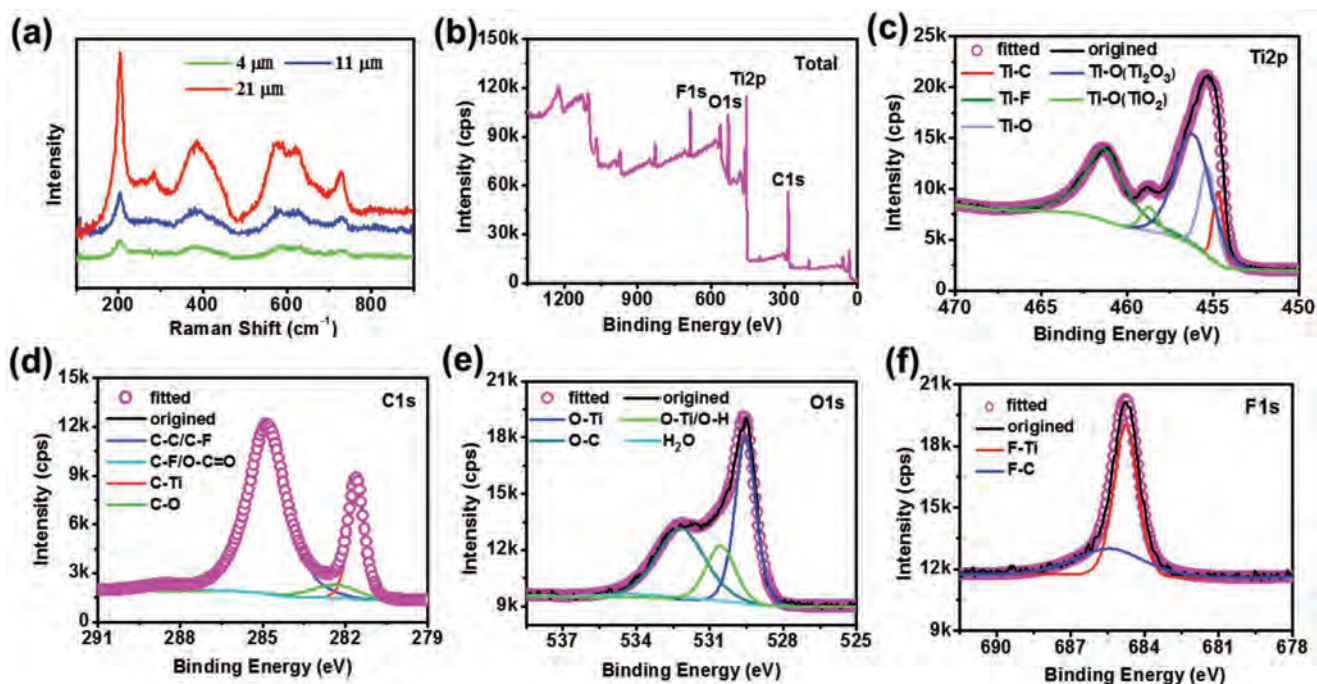


Figure 3. The structural information of atomic composition and bonding of freestanding MXene films. a) Raman spectra recorded from three different MXene films with thickness of $4.0 \pm 0.1 \mu\text{m}$ (green), $11.0 \pm 0.1 \mu\text{m}$ (blue), and $21.0 \pm 0.1 \mu\text{m}$ (red). b) XPS full spectrum of MXene film. Deconvoluted high-resolution XPS spectra of c) $\text{Ti}2p$, d) $\text{C}1s$, e) $\text{O}1s$, and f) $\text{F}1s$.

MXene layers cannot be completely removed by vacuum drying at 200 °C, the trapped water increased when the thickness of MXene films increased.^[37] An apparent vibration mode with $E_g = 280 \text{ cm}^{-1}$ occurred at thicker MXene film with thickness of 21 μm , indicating that the terminal group ratio of OH increases with increasing the thickness of the MXene membrane.

Further, XPS full-scan spectra of MXene film and deconvolution peak fittings for Ti 2p, C 1s, O 1s, and F 1s are illustrated in Figure 3b–f. All the responsive peaks for the elemental species as surveyed in Figure 3b are tabulated (Table S4, Supporting Information). The high-resolution spectrum of the Ti 2p region (Figure 3c) was fitted by components corresponding to the following three species: Ti–C, Ti–F, Ti–O in the forms of Ti–O, Ti_2O_3 , and TiO_2 .^[40] With the replacement of Al elements by more electronegative surface terminations such as O, OH, and F, the binding energies (BE) of the Ti–C species (Ti 2p_{3/2}, 2p_{1/2}) shift to higher BE of 456.2 and 461.4 eV in comparison with their parent MAX phases. Figure 3d shows high-resolution spectrum in the C 1s region that was fitted by components corresponding to C–C, C–Ti, C–OH, COO, and C–F species.^[11,41–43] Figure 3e plots the high-resolution spectrum in the O 1s region which was fitted by components corresponding to the following species: O–C, O–Ti, O–H, and H_2O .^[44,45] The H_2O may be originated from surface oxidation. The high-resolution spectrum in the F 1s region (Figure 3f) was fitted by two components at BE of 684.8 and 685.4 eV, which probably correspond to Ti–F and C–F. Based on deconvolution fitted results, the atomic percentages of Ti, C, O, and F for freestanding MXene membrane are 32.4%, 35.6%, 19.9%, and 12.1%, respectively. Therefore, it is easy to conclude that there are lots of oxygen-containing groups existing in the films, which are beneficial to introducing pseudocapacitance.

To explore the practical applications of freestanding MXene membranes in flexible, mountable, and portable energy-storage devices, we assembled freestanding $\text{Ti}_3\text{C}_2\text{T}_x$ films into flexible solid-state MSCs, as illustrated in Figure 4a. These flexible solid-state MSCs consisted of MXene-based interdigitated electrodes patterned by cold ultraviolet (355 nm) laser processing and PVA/ H_2SO_4 gel electrolyte. And the devices are further supported by a thin polyethylene terephthalate (PET) substrate coated with an Au layer and finally encapsulated by polydimethylsiloxane (PDMS) with excellent flexibility. The as-fabricated micro-supercapacitors with MXene thickness of 11 μm were tested by cyclic voltammetry (CV) at various scan rates ranging from 5 to 100 mV s^{-1} (Figure 4b). As a result, these flexible solid-state MSCs show nearly rectangular CV profiles up to 100 mV s^{-1} , indicating excellent charge storage characteristics and rapid response time. On the one hand, this superior rate-capability ascribes to high electrical conductivity of the MXene films, on the other hand, the coplanar interdigital form utilized here can be helpful for free movement of electrolyte ions and hence leading to better rate capability over their sandwich counterparts. Since the micro-supercapacitors are constructed with thin-film MXene electrodes (the thickness ranges from 1–21 μm) and the intentionally tailored voids between each single interdigital slice, the wettability of the solid-state electrolyte and the transfer length of electrolyte ions can be largely shortened, which is beneficial to improve the rate-capability of micro-supercapacitors although they are based on freestanding MXene films. Moreover, the flexible solid-state

MSCs were further subjected to mechanical bending tests (the inset of Figure 4d). The device shows no capacitance decline upon bending to 60° (Figure 4d). From Figure 4c, the areal capacitances of the devices at different current densities are calculated from galvanostatic charge–discharge (GCD) curves that are 134, 123, 118, 103, and 90 mF cm^{-2} at 0.25, 0.5, 1.0, 2.5, and 5.0 mA cm^{-2} based on the two electrodes, respectively.

As shown in Figure 4e, it is obviously observed that the capacitances like areal and volumetric depend strongly on the thickness of freestanding MXene films. The areal capacitances of up to 73, 134, and 340 mF cm^{-2} can be achieved by using GCD curves when the thickness of the MXene films are 4, 11, and 21 μm , respectively (Figure 4f). According to Equation (2), the corresponding volumetric capacitances are very easily calculated to be 183, 122, and 162 F cm^{-3} , respectively (Figure 4g). At the same time, the typical GCD curves at different current densities are also shown in Figure S9 (Supporting Information). Furthermore, the corresponding areal and volumetric capacitances reach up to 292 mF cm^{-2} and 732 F cm^{-3} when calculated based on only single electrode, which are on the very top level for all the MSCs. To demonstrate the superiority of the aforementioned freestanding MXene electrodes, we compare the areal and volumetric capacitances for freestanding MXene-based flexible solid-state MSCs than other unconventional supercapacitors, as shown in Figure 4h,i, respectively.^[9,22,32,33,46–64] Meanwhile, the detailed information of the areal and volumetric capacitances for MSCs based on other different materials was listed in Table S5 (Supporting Information). Evidently, the excellent areal and volumetric capacitance verifies the high efficiency of $\text{Ti}_3\text{C}_2\text{T}_x$ films in playing high-performance MSCs electrode. And these superior properties can be attributed to resulting change of the valence of the transition metal and the outstanding electrical conductivity, and eventually resulting in fast and reversible redox reactions involving proton intercalation.^[65] Furthermore, the interdigital electrode and larger interlayer spacing as discussed in high resolution transmission electron microscopy (HRTEM) section will further facilitate the ion transfer and diffusion.

Energy and power densities are another two pivotal parameters for freestanding MXene-based flexible solid-state MSCs. As shown in Figure 4i, the highest areal and volumetric energy densities reach up to 43.5 mWh cm^{-2} and 12.4 mWh cm^{-3} at power densities of 87.5 mW cm^{-2} and 218.8 mW cm^{-3} , respectively, which are substantially higher than the other micro-supercapacitors based on activated carbon nanotube (CNT)/graphene,^[48] carbon,^[50] PANI,^[62] and graphene.^[63] Additionally, due to the imperfect packaging process of device, the cycling stability of MXene-based flexible solid-state MSCs performed not very well (Figure S10, Supporting Information). As demonstrated, the capacitance maintains 82.5% over the course of 5000 cycles at GCD current density of 10 mA cm^{-2} . The electrochemical performance of the freestanding MXene-based flexible solid-state MSCs unambiguously indicates the potential of flexible, mountable, and portable energy-storage application.

The extraordinary performance of flexible solid-state MSCs in PVA/ H_2SO_4 gel electrolyte is ascribed to the synergistic combination of elaborated selection of extrahighly conductive freestanding 2D MXene film, simplified device manufactured process, massively cold laser production of interdigital electrodes, and

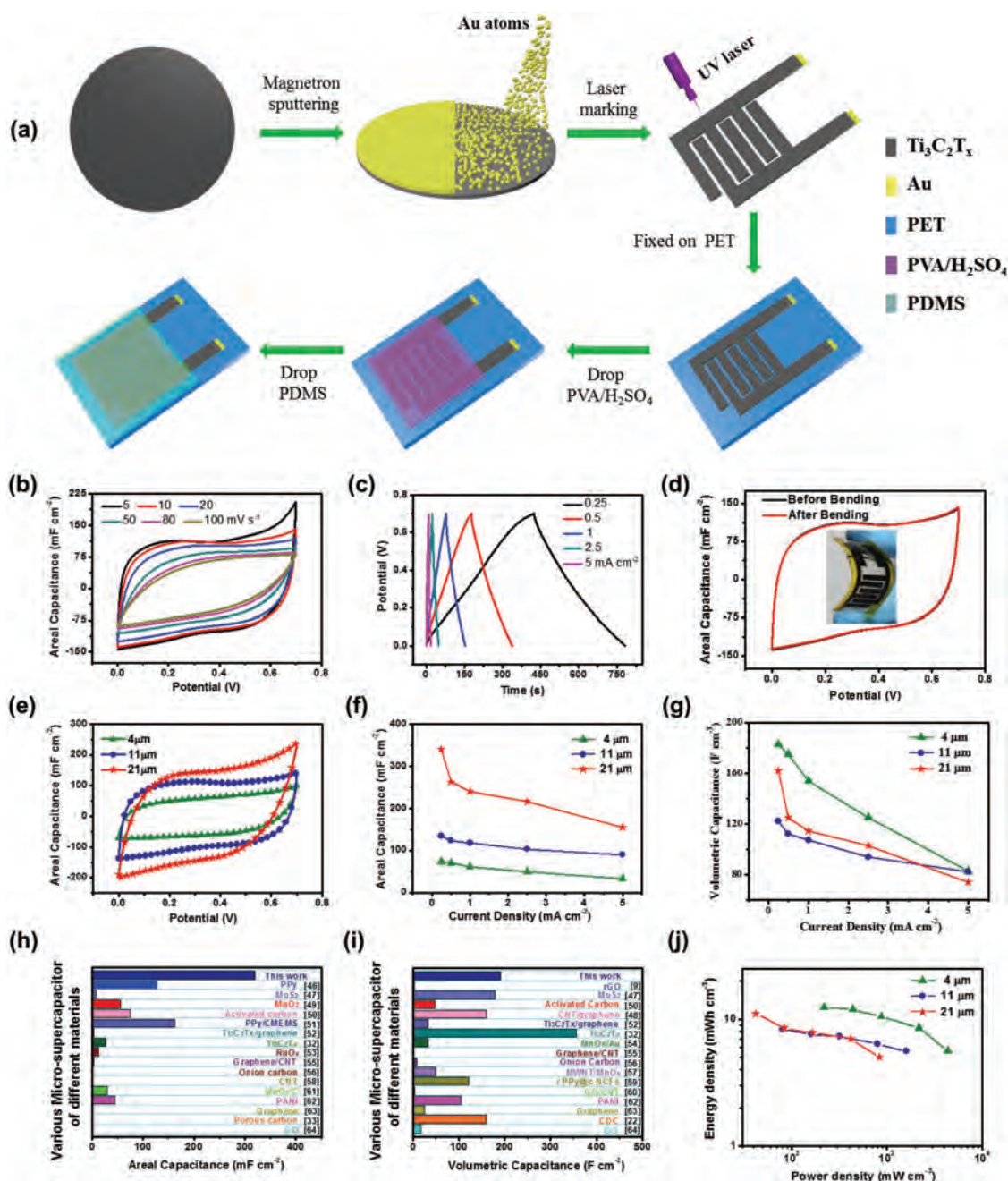


Figure 4. Electrochemical properties of freestanding MXene films based flexible solid-state microsupercapacitors. a) Schematic illustration of manufacturing flexible solid-state microsupercapacitors. b) CV curves at the scan rates varying from 5 to 100 mV s^{-1} . c) GCD curves at different charge–discharge current densities. d) CV curves at 10 mV s^{-1} for microsupercapacitors with interdigital electrode thickness of 11 μm . The inset shows the flexibility of MXene-based microsupercapacitors after bending. e) The corresponding CV curves at 5 mV s^{-1} with different MXene film thicknesses. f) The areal capacitances of flexible solid-state microsupercapacitors with different MXene film thicknesses depend on different current densities. g) The volumetric capacitances of flexible solid-state microsupercapacitors with different MXene film thicknesses depend on different current densities. h) Comparing to the areal capacitances of freestanding MXene films based microsupercapacitors than other devices. i) Comparing to the volumetric capacitances of freestanding MXene films based microsupercapacitors than other devices. j) The Ragone plots.

uncomplicated encapsulation technology of self-flowed PDMS thin film. First, the flexible freestanding 2D MXenes greatly provide the multifunctional improvements for energy storage. The wide interlayer spacing (up to 2.04 nm) of MXene film offers more ionic accommodation and fast transport pathway,

while extrahighly conductive MXenes film acts as main flexible mechanical skeleton and high-speed electron transport network, efficiently guaranteeing the extrahigh areal and volumetric capacitances, energy, and power density of flexible solid state MSCs. Second, the simplified and rapid device manufacture of flexible

solid-state MSCs can effectively boost its massive production and dramatically promote its commercial applications. This low cost fabricated technology can efficiently avoid the complex and expensive process of the other technology, such as multiple-step lithographic manufacturing, plasma etching, and photoresist. Especially, the cold laser (355 nm) process can forcefully guarantee the edge effect of interdigital electrodes without unavoidable ablation from high power hot lasers (1064 nm) and then result in the high performance of MSCs. Third, the strong coupling effect of both the coplanar interdigital electrodes without need of a separator and the unique anisotropy of 2D MXenes film can also make sure the fast ion transport across gel electrolyte and dramatically improve the power intensity of MSCs. Fourth, this binder-free and conductive agent-free freestanding MXene electrode is another key factor to obtain extremely high areal and volumetric capacitances of MSCs. For traditional electrode, the binder has to be employed to improve the mechanical properties but inevitably sacrifice the electrical conductivity of electrode. However, our binder-free MXene electrode possesses not only the excellently flexible mechanical behavior but also extrahigh electrical conductivity (up to $1.25 \times 10^5 \text{ S m}^{-1}$). Last but not least, the self-flowed encapsulation technology of PDMS mounted on the gel electrolyte can easily realize the integration of MSCs into on-chip integrated circuits, especially, for portably wearable flexible electronics.

3. Conclusions

In summary, this work paves a pathway for preparing freestanding conductive thickness-controlled MXene films constructed with 2D platelets by vacuum filtration of MXene aqueous inks. This massive production method in combination with simplified device manufactured process and uncomplicated encapsulation technology unambiguously guarantees the potential application of freestanding highly conductive MXene films and hence opens up a new approach for high performance energy storage devices application in integrated energy management electronics. We demonstrate that freestanding MXene films are promising as active electrodes for energy storage. Significantly, freestanding conductive $\text{Ti}_3\text{C}_2\text{T}_x$ based flexible solid-state micro-supercapacitors with interdigital electrodes and PVA/ H_2SO_4 gel electrolyte display outstanding areal capacitance of 340 mF cm^{-2} , volumetric capacitance of 183 F cm^{-3} , and corresponding energy density of 12.4 mWh cm^{-3} based on the two working electrodes, which are on the topmost level among all the unconventional supercapacitors. And while based on one single electrode for MSCs, the value can reach up to 1360 mF cm^{-2} and 732 F cm^{-3} . To our knowledge, this is the highest volumetric performance for flexible solid-state MSCs. The present work thus establishes MXene films as state-of-the-art electrodes for MSCs, whose performance can be tuned both from a material perspective, given the established synthetic versatility of MXenes, and from an engineering perspective, with the systematic improvement of novel device architectures. We believe that freestanding conductive thickness-controlled MXene films based on solution processable aqueous ink of MXene is promising to target a broad variety of applications such as storage, sensing, catalysis, shielding, and purification.

4. Experimental Section

Preparation of Water-Stable MXene Colloidal Solutions: The preparation of Ti_3AlC_2 powders was reported elsewhere.^[34] Briefly, titanium (99%, GRINM, China), aluminum (99%, GRINM, China), and carbon black (99%, GRINM, China) powders in a 3:1.2:1.9 molar ratio were first mixed. Then, the mixtures were ball milled and sintered at 1500°C for 5 min in a flowing argon atmosphere through a spark plasma sintering method (FCT, Rauenstein, Germany). For exfoliating, 1.98 g LiF was added to 30 mL 6 M HCl solution, followed by stirring for 10 min to dissolve sufficiently. After that, 1.2 g Ti_3AlC_2 powder was slowly added to the mixture solution in 5 min, followed by stirring at 40°C for 45 h, as described elsewhere.^[30] Then the obtained suspension was washed with deionized water (DI water) and centrifuged repeatedly until the pH of the suspension was above 6.0. Finally, to obtain the MXene $\text{Ti}_3\text{C}_2\text{T}_x$ colloidal solution, a further sonication for 1 h, and then a centrifugation at 3500 rpm for 1 h was processed.

Preparation of Freestanding $\text{Ti}_3\text{C}_2\text{T}_x$ Films: In order to obtain freestanding $\text{Ti}_3\text{C}_2\text{T}_x$ films, vacuum-assisted filtration was utilized. The colloidal aqueous solutions could form uniform $\text{Ti}_3\text{C}_2\text{T}_x$ films on hydrophilic membrane with pore size of $0.2 \mu\text{m}$ and the thickness of the film was adjustable by controlling the amount of colloidal solution. Then, $\text{Ti}_3\text{C}_2\text{T}_x$ films with thickness ranging from 1 to $21 \mu\text{m}$ were prepared after drying at room temperature. Finally, freestanding MXene conductive films could be obtained through removal of the porous membrane.

Characterizations: XRD patterns were obtained with a powder diffractometer (PANalytical X'Pert Powder diffractometer, Holland) using Cu K α radiation and a step scan of 0.02° over a 2θ range of 5° – 80° . A SEM (FEI QUANTA FEG 250, American) was used to obtain high-magnification images of vacuum-dried powders and freestanding films and conduct elemental analysis via EDX spectroscopy. After that, water-stable colloidal solution was directly dropped onto ultrathin carbon supported Cu mesh, and then the 2D sheets were investigated by TEM (JEOL JEM-2100, Japan), with an accelerating voltage of 200 kV. XPS data were recorded with a Thermo Scientific ESCALAB 250Xi spectrometer with chamber pressure maintained in the 10^{-6} – 10^{-7} Pa range during XPS measurements. Raman spectra were obtained from a RM2000 microscopic confocal Raman spectrometer with a 785 nm Ar ions laser beam. The film resistances of freestanding MXene films were measured using a four-probe technique (RTS8, China).

Synthesis of Gel Electrolyte: 8 g concentrated H_2SO_4 with a mass ratio of 98% was carefully and slowly added into 80 mL DI water. Then 8 g PVA (1799 type) were mixed with the H_2SO_4 aqueous solution with cooling down to room temperature. The above-obtained solution was stirred for 1 h in a water bath with the temperature controlled at 80°C . And clear PVA/ H_2SO_4 gel electrolyte was obtained after the solution was cooled down to room temperature.

Fabrication of Flexible Solid-State MSCs: The freestanding MXene films were first covered by a layer of gold plating through magnetron sputtering (TRP450, China). Then, the MXene films were carved into an interdigital pattern with a specific area of 2.25 cm^2 through ultraviolet laser marking technology (UV-3S, China). Third, the film was fixed on a PET film with tape, after that a PVA/ H_2SO_4 gel electrolyte was carefully dropped onto the patterns. Then the electrode was placed into the mold and fixed with clips until the gel electrolyte was semi-solidified. Finally, the device was packaged with PDMS module glue and left in air for 24 h at room temperature. When the PDMS module glue was curing, through removing the mold, flexible solid-state MSCs were successfully prepared.

Electrochemical Measurements: The CV, GCD, and electrochemical impedance spectroscopy were conducted with a CHI 660E electrochemical workstation (Chenhua, Shanghai, China). The cycling stability measurement was carried out on an Arbin MSTAT4 multichannel galvanostat/potentiostat instrument (Arbin, USA). The areal capacitance (C_A), the volumetric capacitance (C_V), the volumetric energy density (E_V), and the volumetric power density (P_V) were calculated as following

$$C_A = I_s / [(dU/dt) \cdot S] \quad (\text{mF cm}^{-2}) \quad (1)$$

$$C_V = I_s / [(dU/dt) \cdot S \cdot d] \quad (\text{F cm}^{-3}) \quad (2)$$

$$E_V = C_V \cdot V^2 / (2 \times 3.6) \quad (\text{mWh cm}^{-3}) \quad (3)$$

$$P_V = 3.6 E_V / \Delta t \quad (\text{mW cm}^{-3}) \quad (4)$$

where I_s is GCD charge–discharge current density based on the areal parameter, Δt is GCD discharge time after the IR drop, dU/dt indicates the slope of these GCD curves, which is very close to its mean value when the GCD curve is approximately linear; S is the efficient area of the two interdigital electrodes, and d is the MXene film thickness, and V is potential window, respectively.

Supporting Information

Supporting Information is available from the Wiley Online Library or from the author.

Acknowledgements

H.H. and H.S. contributed equally to this work. This work was financially supported by the National Natural Science Foundation of China (Grant No. 51602265), the Independent Research Project of State Key Laboratory of Traction Power (Grant Nos. 2017TPL_Z04 and 2016TPL_Z03), and the Fundamental Research Funds for the Central Universities of China (Grant Nos. 2682016CX074, 2682017CY06, 2682016ZY01, and 2682017ZDYP01).

Conflict of Interest

The authors declare no conflict of interest.

Keywords

areal and volumetric properties, flexible solid-state devices, freestanding conductive films, micro-supercapacitors, MXenes

Received: March 22, 2018

Revised: May 6, 2018

Published online:

- [1] D. S. Yu, Q. H. Qian, L. Wei, W. C. Jiang, K. L. Goh, J. Wei, J. Zhang, Y. Chen, *Chem. Soc. Rev.* **2015**, *44*, 647.
- [2] L. L. Liu, Z. Q. Niu, J. Chen, *Chem. Soc. Rev.* **2016**, *45*, 4340.
- [3] B. Anasori, M. R. Lukatskaya, Y. Gogotsi, *Nat. Rev. Mater.* **2017**, *2*, 16098.
- [4] L. Jin, J. Chen, B. Zhang, W. Deng, L. Zhang, H. Zhang, X. Huang, M. Zhu, W. Yang, Z. L. Wang, *ACS Nano* **2016**, *10*, 7874.
- [5] L. Jin, W. Deng, Y. Su, Z. Xu, H. Meng, B. Wang, H. Zhang, B. Zhang, L. Zhang, X. Xiao, M. Zhu, W. Yang, *Nano Energy* **2017**, *38*, 185.
- [6] P. Huang, C. Lethien, S. Pinaud, K. Brousse, R. Laloo, V. Turq, M. Respaud, A. Demortiere, B. Daffos, P. L. Taberna, B. Chaudret, Y. Gogotsi, P. Simon, *Science* **2016**, *351*, 691.
- [7] M. F. El-Kady, M. Ihms, M. P. Li, J. Y. Hwang, M. F. Mousavi, L. Chaney, A. T. Lech, R. B. Kaner, *Proc. Natl. Acad. Sci. USA* **2015**, *112*, 4233.
- [8] D. Pech, M. Brunet, H. Durou, P. H. Huang, V. Mochalin, Y. Gogotsi, P. L. Taberna, P. Simon, *Nat. Nanotechnol.* **2010**, *5*, 651.
- [9] M. F. El-Kady, V. Strong, S. Dubin, R. B. Kaner, *Science* **2012**, *335*, 1326.
- [10] Y. Zhang, W. Y. Bai, X. L. Cheng, J. Ren, W. Weng, P. N. Chen, X. Fang, Z. T. Zhang, H. S. Peng, *Angew. Chem., Int. Ed.* **2014**, *53*, 14564.
- [11] K. Wang, X. Zhang, C. Li, X. Z. Sun, Q. H. Meng, Y. W. Ma, Z. X. Wei, *Adv. Mater.* **2015**, *27*, 7451.
- [12] W. C. Jiang, S. L. Zhai, Q. H. Qian, Y. Yuan, H. E. Karahan, L. Wei, K. L. Goh, A. K. Ng, J. Wei, Y. Chen, *Energy Environ. Sci.* **2016**, *9*, 611.
- [13] J. J. Yoo, K. Balakrishnan, J. S. Huang, V. Meunier, B. G. Sumpter, A. Srivastava, M. Conway, A. L. M. Reddy, J. Yu, R. Vajtai, P. M. Ajayan, *Nano Lett.* **2011**, *11*, 1423.
- [14] X. Xiao, T. Q. Li, P. H. Yang, Y. Gao, H. Y. Jin, W. J. Ni, W. H. Zhan, X. H. Zhang, Y. Z. Cao, J. W. Zhong, L. Gong, W. C. Yen, W. J. Mai, J. Chen, K. F. Huo, Y. L. Chueh, Z. L. Wang, J. Zhou, *ACS Nano* **2012**, *6*, 9200.
- [15] M. Beidaghi, Y. Gogotsi, *Energy Environ. Sci.* **2014**, *7*, 867.
- [16] H. T. Zhang, H. Su, L. Zhang, B. B. Zhang, F. J. Chun, X. Chu, W. D. He, W. Q. Yang, *J. Power Sources* **2016**, *331*, 332.
- [17] Y. Y. Peng, B. Akuzum, N. Kurra, M. Q. Zhao, M. Alhabe, B. Anasori, E. C. Kumbur, H. N. Alshareef, M. D. Ger, Y. Gogotsi, *Energy Environ. Sci.* **2016**, *9*, 2847.
- [18] Q. Jiang, C. Wu, Z. Wang, A. C. Wang, J. H. He, Z. L. Wang, H. N. Alshareef, *Nano Energy* **2018**, *45*, 266.
- [19] W. Yang, L. He, X. C. Tian, M. Y. Yan, H. Yuan, X. B. Liao, J. S. Meng, Z. M. Hao, L. Q. Mai, *Small* **2017**, *13*, 1700639.
- [20] M. F. El-Kady, R. B. Kaner, *Nat. Commun.* **2013**, *4*, 1475.
- [21] N. A. Kyeremateng, T. Brousse, D. Pech, *Nat. Nanotechnol.* **2017**, *12*, 7.
- [22] J. Chmiola, C. Largeot, P. L. Taberna, P. Simon, Y. Gogotsi, *Science* **2010**, *328*, 480.
- [23] Y. Sun, D. Chen, Z. Liang, *Mater. Today Energy* **2017**, *5*, 22.
- [24] M. Naguib, V. N. Mochalin, M. W. Barsoum, Y. Gogotsi, *Adv. Mater.* **2014**, *26*, 992.
- [25] M. Naguib, O. Mashtalir, J. Carle, V. Presser, J. Lu, L. Hultman, Y. Gogotsi, M. W. Barsoum, *ACS Nano* **2012**, *6*, 1322.
- [26] J. Halim, S. Kota, M. R. Lukatskaya, M. Naguib, M. Q. Zhao, E. J. Moon, J. Pitock, J. Nanda, S. J. May, Y. Gogotsi, M. W. Barsoum, *Adv. Funct. Mater.* **2016**, *26*, 3118.
- [27] P. Urbankowski, B. Anasori, T. Makaryan, D. Q. Er, S. Kota, P. L. Walsh, M. Q. Zhao, V. B. Shenoy, M. W. Barsoum, Y. Gogotsi, *Nanoscale* **2016**, *8*, 11385.
- [28] T. L. Tan, H. M. Jin, M. B. Sullivan, B. Anasori, Y. Gogotsi, *ACS Nano* **2017**, *11*, 4407.
- [29] Q. Jiang, N. Kurra, M. Alhabe, Y. Gogotsi, H. N. Alshareef, *Adv. Energy Mater.* **2018**, *7*, 1703043.
- [30] M. Ghidui, M. R. Lukatskaya, M. Q. Zhao, Y. Gogotsi, M. W. Barsoum, *Nature* **2014**, *516*, 78.
- [31] B. Mendoza-Sánchez, Y. Gogotsi, *Adv. Mater.* **2016**, *28*, 6104.
- [32] B. Hsia, J. Marschewski, S. Wang, J. B. In, C. Carraro, D. Poulidakos, C. P. Grigoropoulos, R. Maboudian, *Nanotechnology* **2014**, *25*, 055401.
- [33] J. B. In, B. Hsia, J.-H. Yoo, S. Hyun, C. Carraro, R. Maboudian, C. P. Grigoropoulos, *Carbon* **2015**, *83*, 144.
- [34] C. Wang, T. Yang, S. Kong, J. Xiao, J. Xue, Q. Wang, C. Hu, Q. Huang, Y. Wang, *J. Nucl. Mater.* **2013**, *440*, 606.
- [35] P. Simon, *ACS Nano* **2017**, *11*, 2393.
- [36] O. Mashtalir, M. Naguib, V. N. Mochalin, Y. Dall'Agnese, M. Heon, M. W. Barsoum, Y. Gogotsi, *Nat. Commun.* **2013**, *4*, 1716.
- [37] M. A. Hope, A. C. Forse, K. J. Griffith, M. R. Lukatskaya, M. Ghidui, Y. Gogotsi, C. P. Grey, *Phys. Chem. Chem. Phys.* **2016**, *18*, 5099.
- [38] S. Kajiyama, L. Szabova, K. Sodeyama, H. Iinuma, R. Morita, K. Gotoh, Y. Tateyama, M. Okubo, A. Yamada, *ACS Nano* **2016**, *10*, 3334.

- [39] T. Hu, J. M. Wang, H. Zhang, Z. J. Li, M. M. Hu, X. H. Wang, *Phys. Chem. Chem. Phys.* **2015**, *17*, 9997.
- [40] J. Yan, C. E. Ren, K. Maleski, C. B. Hatter, B. Anasori, P. Urbankowski, A. Sarycheva, Y. Gogotsi, *Adv. Funct. Mater.* **2017**, *27*, 1701264.
- [41] H. Su, H. Zhang, F. Liu, F. Chun, B. Zhang, X. Chu, H. Huang, W. Deng, B. Gu, H. Zhang, X. Zheng, M. Zhu, W. Yang, *Chem. Eng. J.* **2017**, *322*, 73.
- [42] H. Zhang, L. Zhang, J. Chen, H. Su, F. Liu, W. Yang, *J. Power Sources* **2016**, *315*, 120.
- [43] H. T. Zhang, X. Zhang, X. Z. Sun, Y. W. Ma, *Sci. Rep.* **2013**, *3*, 3534.
- [44] H. T. Zhang, X. Zhang, X. Z. Sun, D. C. Zhang, H. Lin, C. H. Wang, H. J. Wang, Y. W. Ma, *ChemSusChem* **2013**, *6*, 1084.
- [45] H. T. Zhang, X. Zhang, D. C. Zhang, X. Z. Sun, H. Lin, C. H. Wang, Y. W. Ma, *J. Phys. Chem. B* **2013**, *117*, 1616.
- [46] W. Sun, R. Zheng, X. Chen, *J. Power Sources* **2010**, *195*, 7120.
- [47] L. Cao, S. Yang, W. Gao, Z. Liu, Y. Gong, L. Ma, G. Shi, S. Lei, Y. Zhang, S. Zhang, R. Vajtai, P. M. Ajayan, *Small* **2013**, *9*, 2905.
- [48] H. R. Byon, S. W. Lee, S. Chen, P. T. Hammond, Y. Shao-Horn, *Carbon* **2011**, *49*, 457.
- [49] X. Wang, B. D. Myers, J. Yan, G. Shekhawat, V. Dravid, P. S. Lee, *Nanoscale* **2013**, *5*, 4119.
- [50] M. Beidaghi, W. Chen, C. Wang, *J. Power Sources* **2011**, *196*, 2403.
- [51] M. Beidaghi, C. Wang, *Electrochim. Acta* **2011**, *56*, 9508.
- [52] H. Li, Y. Hou, F. Wang, M. R. Lohe, X. Zhuang, L. Niu, X. Feng, *Adv. Energy Mater.* **2017**, *7*, 1601847.
- [53] S. Makino, Y. Yamauchi, W. Sugimoto, *J. Power Sources* **2013**, *227*, 153.
- [54] W. Si, C. Yan, Y. Chen, S. Oswald, L. Han, O. G. Schmidt, *Energy Environ. Sci.* **2013**, *6*, 3218.
- [55] J. Lin, C. Zhang, Z. Yan, Y. Zhu, Z. Peng, R. H. Hauge, D. Natelson, J. M. Tour, *Nano Lett.* **2013**, *13*, 72.
- [56] D. Pech, M. Brunet, H. Durou, P. Huang, V. Mochalin, Y. Gogotsi, P. L. Taberna, P. Simon, *Nat. Nanotechnol.* **2010**, *5*, 651.
- [57] G. Lee, D. Kim, J. Yun, Y. Ko, J. Cho, J. S. Ha, *Nanoscale* **2014**, *6*, 9655.
- [58] P. You-Yu, A. Bilen, K. Narendra, Z. Meng-Qiang, A. Mohamed, A. Babak, K. Emin Caglan, A. Husam N, G. Ming-Der, G. Yury, *Energy Environ. Sci.* **2016**, *9*, 9200.
- [59] Z. Wang, D. O. Carlsson, P. Tammela, K. Hua, P. Zhang, L. Nyholm, M. Strømme, *ACS Nano* **2015**, *9*, 7563.
- [60] F. Wen, C. Hao, J. Xiang, L. Wang, H. Hou, Z. Su, W. Hu, Z. Liu, *Carbon* **2014**, *75*, 236.
- [61] C. Shen, X. Wang, S. Li, J. g. Wang, W. Zhang, F. Kang, *J. Power Sources* **2013**, *234*, 302.
- [62] C. Meng, J. Maeng, S. W. M. John, P. P. Irazoqui, *Adv. Energy Mater.* **2014**, *4*, 1301269.
- [63] Z. S. Wu, K. Parvez, X. Feng, K. Müllen, *J. Mater. Chem. A* **2014**, *2*, 8288.
- [64] Z. S. Wu, K. Parvez, X. Feng, K. Mullen, *Nature. Commun.* **2013**, *4*, 2487.
- [65] M. R. Lukatskaya, S. M. Bak, X. Q. Yu, X. Q. Yang, M. W. Barsoum, Y. Gogotsi, *Adv. Energy Mater.* **2015**, *5*, 1500589.